AGU PUBLICATIONS

JGR

Journal of Geophysical Research: Atmospheres

RESEARCH ARTICLE

10.1002/2016JD025268

Atmospheric structure favoring high sea surface temperatures in the western equatorial Pacific

Anindya Wirasatriya[1,2], Hiroshi Kawamura[3], Teruhisa Shimada[4], and Kohtaro Hosoda[3]

[1]Department of Oceanography, Faculty of Fisheries and Marine Sciences, Diponegoro University, Semarang, Indonesia, [2]Center for Coastal Disaster Mitigation and Rehabilitation Studies, Diponegoro University, Semarang, Indonesia, [3]Center for Atmospheric and Oceanic Studies, Graduate School of Science, Tohoku University, Sendai, Japan, [4]Faculty of Science and Technology, Hirosaki University, Hirosaki, Japan

Key Points:

- The suppressed phase of MJO may also contribute for the development of HE
- The suppressed convection generated from the deep convection outside of HE area increase solar radiation during the development stage
- During the development and decay stage of HE, the variability of convection at the upper layer is influenced by surface wind

Correspondence to:
A. Wirasatriya,
aninosi@yahoo.co.id

Citation:
Wirasatriya, A., H. Kawamura, T. Shimada, and K. Hosoda (2016), Atmospheric structure favoring high sea surface temperatures in the western equatorial Pacific, *J. Geophys. Res. Atmos.*, *121*, 11,368–11,381, doi:10.1002/2016JD025268.

Received 24 APR 2016
Accepted 13 SEP 2016
Accepted article online 15 SEP 2016
Published online 8 OCT 2016

Abstract We investigated the atmospheric processes over high sea surface temperature called Hot Event (HE) in the western equatorial Pacific from climatological analysis and a case study of the HE which began on 28 May 2003 (hereafter, HE030528). Climatological analysis shows that during the development stage of HE, solar radiation inside the HE area is higher than its climatology and wind speed is lower than the decay stage. During the decay stage, strong westerly wind often occurs inside HE area. The case study of HE030528 shows that the suppressed convection above high SST area resulted from the deep convection from the northern and southern areas outside HE. The suppressed convection created a band-shaped structure of low cloud cover along HE area increasing solar radiation during the development stage. Thus, the theory of "remote convection" was supported for the HE030528 formation mechanisms. The large sea level pressure gradient magnitude between the southern side of the terrain gap and the northern coast of the Solomon Islands, through which strong wind blew, indicated the role of land topography for the increase of wind speed during the decay of HE030528. Moreover, surface wind had an important role to influence the variability of solar radiation during the occurrence of HE030528 by controlling the water vapor supply in the upper troposphere through surface evaporation and surface convergence variation. Thus, surface wind was the key factor for HE030528 occurrence. The representativeness of HE030528 and the possible relation between HE and Madden-Julian Oscillation are also discussed.

1. Introduction

The occurrence of high sea surface temperature (SST) in the tropical regions has attracted researchers to investigate the mechanisms since the formation of high SST requires a particular atmospheric process [e.g., *Ramanathan and Collins*, 1991; *Wallace*, 1992; *Arking and Ziskin*, 1994; *Tompkins*, 2001]. This process is depicted by *Waliser and Graham* [1993] which shows the relation between SSTs and deep convection. They used highly reflective cloud data obtained from the subjective analysis of daily visible and infrared daily satellite images and monthly SST data with a grid interval of 2° generated from blended satellite observation and in situ data. As the SST increases from 26°C to 29.5°C, highly reflective cloud also increases. Conversely, in the range between 29.5°C and 32°C, the highly reflective cloud decreases with the increase of SST. Thus, the analysis provided evidence that different atmospheric processes affect SSTs below and above 29.5°C.

The well-organized region with high SST of more than 30°C in the tropics has been studied from satellite observations [*Qin et al.*, 2007; *Kawamura et al.*, 2008; *Qin and Kawamura*, 2009a]. *Qin et al.* [2007] named those phenomena as the Hot Event (HE). Using daily and 0.1° × 0.1° satellite SST product, they found that the HE occurrence in the equatorial region is generated under the condition of high solar radiation and low wind speed with high amplitude of diurnal SST variations. *Kawamura et al.* [2008] provided the observational evidence for large amplitude of diurnal SST and *Qin and Kawamura* [2009a] showed the heat gain into the ocean during HE occurrence.

Focusing the study area on the western equatorial Pacific, *Qin et al.* [2008], *Qin and Kawamura* [2009b, 2010], and *Chen and Qin* [2016] investigated the air-sea interaction processes underlying the occurrence of SST of more than 30°C in November 2006. They named this Hot Event as HE0611. They indicated that the high solar radiation during the HE occurrence is controlled by the "remote convection" mechanism associated with a subsurface high-temperature anomaly that occurs during an El Niño event. The "remote convection" mechanisms have been described schematically by *Tompkins* [2001] based on an idealized

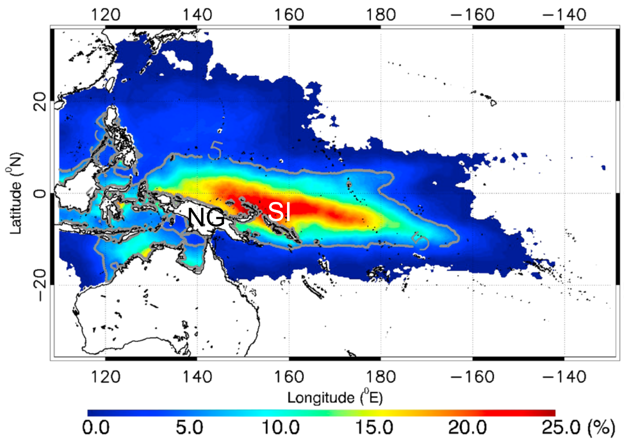

Figure 1. Occurrence frequency of HEs (%) from 2003 to 2011 (100% is 3163 days; ≈ 9 year period). The *gray contour* represents the occurrence rate of 5% used for statistical analysis described in section 2. "NG" and "SI" are the New Guinea Island and the Solomon Island, respectively [modified from *Wirasatriya et al*., 2015].

3-D experiment of cloud-resolving model. The mechanism explains on how SST increases up to 32°C in the equatorial region. The deep convection generates the circulation that sinks air in the remote area and then increases the SST. Moreover, he emphasized that surface latent heat flux limits SSTs to 32°C at most. Eventually, the convection is attracted to propagate toward the high-SST areas, reducing SSTs. *Qin and Kawamura* [2010] first presented the observational evidence of "remote convection" by using data from a geostationary meteorological satellite, and *Chen and Qin* [2016] explained the detailed process.

Wirasatriya et al. [2015] elaborated on the climatology of HEs in the western equatorial Pacific using SST data set derived from satellite microwave sensors. Instead of using constant SST threshold of 30°C for HE identification by *Qin et al*. [2008], *Wirasatriya et al*. [2015] used the SST threshold changing temporally according to daily mean SST inside the area of 27°C. Throughout 9 years observation (2003–2011), they showed that HEs frequently occur along the northern coast of the New Guinea Island and the Solomon Islands extending eastward up to 160°W (Figure 1). This area is collocated with the area of solar radiation more than 200 W/m^2 and wind speed less than 4 m/s in the climatology. The presence of low wind speeds is a key factor in the mechanism for HE occurrence in the western equatorial Pacific. During the HE periods, the solar radiation of more than 200 W/m^2 occurs across much of the equatorial region. In areas where wind speeds are low, latent heat loss is reduced and high SSTs occur, leading to the occurrence of HEs. *Wirasatriya et al*. [2015] also emphasized that the occurrences of high solar radiation and low wind speed are much more common during the development stage and less common during the decay stage.

However, the previous studies on HE has mainly focused the mean state during HE occurrences and paid little attention to the process on how HEs develop and decay. Variations of solar radiation and wind speed were not examined throughout the stages. Thus, this paper is aimed to investigate HE by stages to obtain detailed atmospheric process over the HE area in the western equatorial Pacific. The results clearly show the "remote convection" circulation over an HE area which is different from the "remote convection" circulation proposed by *Qin and Kawamura* [2010]. Our focus on the atmospheric process of HE is independent from El Niño–Southern Oscillation since our HE detection method has excluded the seasonal and interannual effect as explained in *Wirasatriya et al*. [2015].

Data and method are described in section 2. The variabilities of solar radiation and surface wind during the development and decay stages of HE is examined in section 3. We compare "remote convection" mechanisms proposed by the previous studies and shown by this study and discuss possible relationship with the Madden-Julian Oscillation (MJO) in section 4. Conclusion is given in section 5.

2. Data Set and Method

We used the New Generation Sea Surface Temperature for Open Ocean (NGSST-O-Global-V2.0a) to investigate HEs in the western equatorial Pacific. This data set is produced by merging SST observations acquired by two satellite microwave sensors (AMSR-E onboard Aqua and WindSat onboard Coriolis). This product is daily SST fields with a grid interval of 0.25°. Optimal interpolation technique was applied for merging, using decorrelation scales derived by *Hosoda* [2015]. Before the data merging, diurnal correction was applied to estimate 1 m depth SST at the local time of dawn (06:00 LT) at each longitude [*Hosoda*, 2013]. The bias and

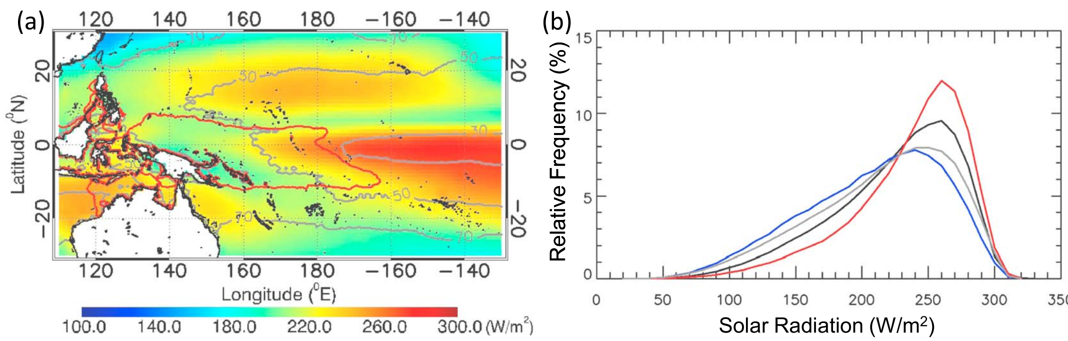

Figure 2. (a) Climatology of solar radiation in the western equatorial Pacific (2003–2011). The gray contour denotes its standard deviation and the red contour represents the frequent HE area with the occurrence rate of more than 5% (See Figure 1). (b) Relative frequency of solar radiation with a discrete interval 10 W/m^2 for inside HE area during the development stage of HE (red line), inside HE area during HE period (black line), inside HE area during the decay stage of HE (blue line), and inside frequent HE area (i.e., red contour in Figure 2a) from 2003 to 2011 (gray line).

root-mean-square error of the merged SST against the TAO/TRITON buoy SST in the study area are −0.107°C and 0.428°C, respectively. Description on this data set was given by *Hosoda and Sakaida* [2015]. The examination of this data set for detecting HE is explained in *Wirasatriya et al*. [2015].

We analyzed the atmospheric effect and response during the development and decay stages of HEs by using the variables from 6-hourly reanalysis data by the Japanese 55 year Reanalysis (JRA55) [*Kobayashi et al*., 2015] for 2003–2011. The data are provided on a 1.25° horizontal grid. The data set contains 37 isobaric surfaces. We used cloud cover, convective heating rate, vertical velocity, divergence, relative humidity, surface wind, sea level pressure (SLP), surface evaporation, and surface precipitation. We calculated surface divergence from the surface wind data. Additionally, we used daily net surface solar radiation on a 1° × 1° grid for 2003–2009 from the International Satellite Cloud Climatology Project (ISCCP) data set [*Zhang et al*., 2004]. These data sets are interpolated onto a 0.25° grid to synchronize with the SST data set. We also used the Global 30 arc sec elevation (GTOPO30) for land elevation data.

The method of this study follows that proposed in *Wirasatriya et al*. [2015]. The HE is defined as a connected region with SST higher than the space-time-dependent threshold of about 30°C, with a minimum areal size of 2×10^6 km, and with a duration period longer than 6 days. The development stage is defined as the period of time from the day when the areal size starts to increase to the day when the areal size reaches its maximum (peak). The decay stage is defined as the period of time from the day when the areal size begins to decrease from the maximum to the day when the areal size reaches its minimum.

We conducted a climatological analysis and a case study. The climatological analysis used 71 HEs identified by *Wirasatriya et al*. [2015] during 2003–2011 in the western equatorial Pacific. The occurrence frequency of the identified HEs is shown in Figure 1. We compared the relative frequencies of atmospheric parameters from 2003 to 2011 inside the area of HE occurrence frequency more than 5% described in Figure 1 and inside the area of individual HE during the development and decay stages. The result of this analysis is then compared to the analysis of the mean state of HE provided in Figure 7 of *Wirasatriya et al*. [2015] and used for case study selection. Case study was conducted to obtain the detail of the atmospheric variation during the development and decay stages of HE. We chose an HE which can represent the general characteristics of HE in the western equatorial Pacific.

3. Results

3.1. Climatological Analysis

Climatological analysis was conducted for solar radiation and surface wind. The variability in solar radiation for all HE cases during the development and decay stages is statistically summarized in Figure 2. Figure 2a shows that the region with the occurrence rate of HE of more than 5% is collocated with solar radiation ~200 W/m^2. However, solar radiation in that area is not stable since the standard deviation is high (>30 W/m^2). Figure 2b shows that the development stage of HE is characterized by the increase of frequency of solar

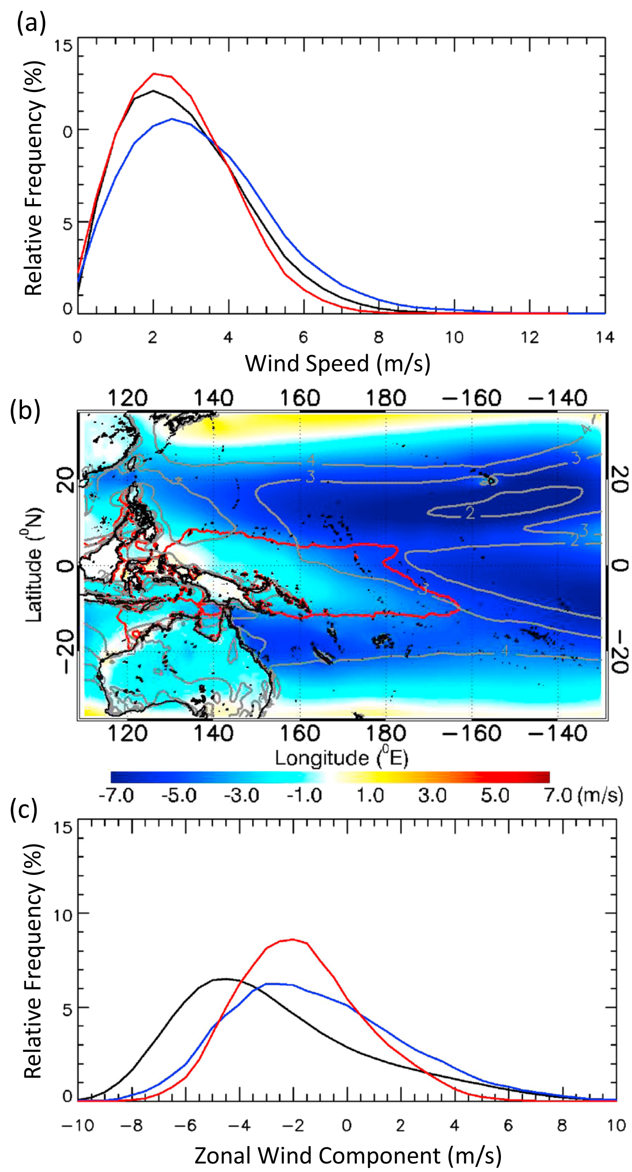

Figure 3. (a) Relative frequency of surface wind speed with discrete interval 0.5 m/s for inside HE area during the development stage of HE (red line), inside HE area during HE period (black line), and inside HE area during the decay stage of HE (blue line). The black line is taken from *Wirasatriya et al.* [2015]. (b) Climatology of zonal surface wind component in the western equatorial Pacific (2003–2011). The gray contour denotes its standard deviation and the red contour represents the frequent HE area with the occurrence rate of more than 5% (See Figure 1). (c) Relative frequency of zonal surface wind component with discrete interval 0.5 m/s for inside HE area during the development stage of HE (red line), inside HE area during the decay stage of HE (blue line), and inside frequent HE area (i.e., red contour in Figure 3a) from 2003 to 2011 (black line).

radiation more than 230 W/m^2 while that of the decay stage is by the increase of frequency of solar radiation less than 230 W/m^2. This indicates that solar radiation is higher during the development stage than decay stage. Moreover, the solar radiation distribution more than 230 W/m^2 for the mean state is located between the development and decay stages. This means that solar radiation more than 230 W/m^2 may cause the development of HE while the occurrence of HE is maintained by the solar radiation of more than 200 W/m^2 as explained in *Wirasatriya et al.* [2015]. Next, the lower solar radiation cause HE to decay. Moreover, comparing to the climatology of solar radiation distribution inside frequent HE area, the relative frequency of climatology is close to the relative frequency during the decay stage. This indicates that during the development stage, solar radiation is higher than its climatology. Therefore, the development stage of HE in the western equatorial Pacific can be characterized by higher solar radiation from its climatology.

The climatological analysis of surface wind is shown in Figure 3. Figure 3a shows that during the development stage of HE, the relative frequency of low wind speed is higher than during the decay stage and the relative frequency of the mean state is in between. The intersection of frequency is at 4 m/s which indicates that the wind speed of less than 4 m/s mostly occurs during the development stage, followed by the mean state, and then the decay stage of HE. Therefore, it can be concluded that the development stage of HE is characterized by the occurrence of weak wind speed while that of the decay stage is by the occurrence of strong wind.

Furthermore, we extended the climatological analysis of surface wind for the zonal component since the occurrence of strong westerly wind inside the HE area was identified during the decay stages of 48 HEs (i.e., 68% of all HE cases). Figure 3b shows that the climatology of the frequent HE area is characterized by the easterly wind with the magnitude of lower than 3 m/s. However, it also corresponds to the area of high

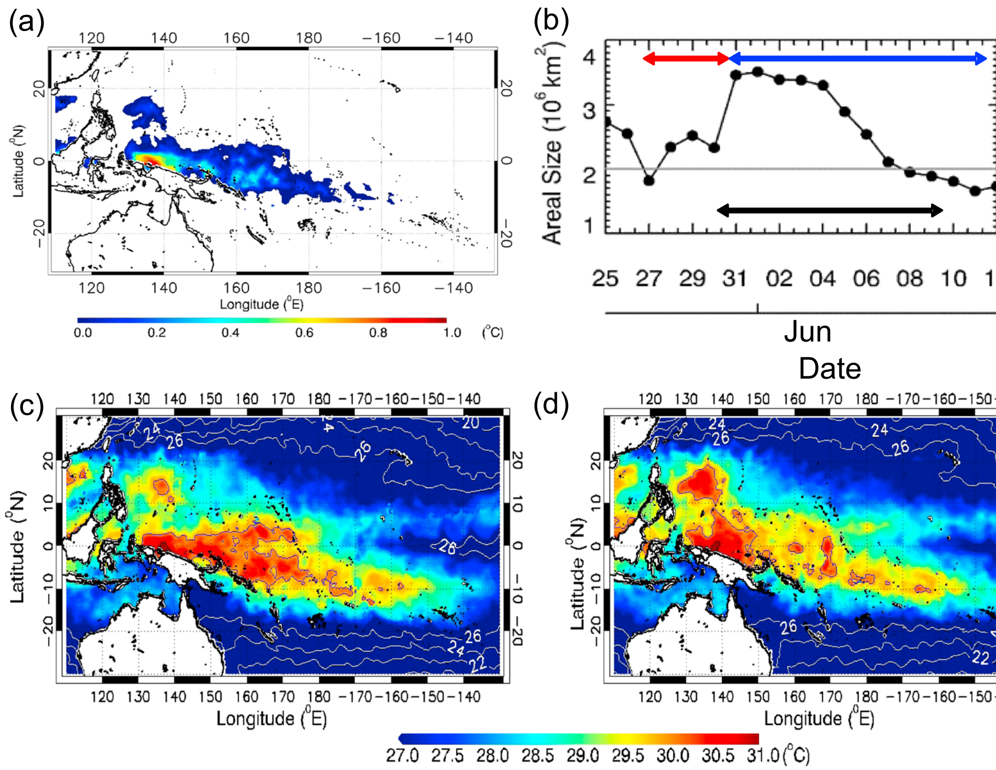

Figure 4. General feature of HE030528. (a) Amplitude map, (b) temporal evolution of areal size of the HE, (c) SST map at the peak of HE (31 May 2003), and (d) SST map at the decay stage of HE (6 June 2003). Amplitude map is the composite of daily amplitude throughout the period of HE030528. Daily amplitude is calculated by subtracting daily SSTs from space-time-dependent threshold as shown in *Wirasatriya et al.* [2015]. The black, red, and blue arrows in Figure 4b denote the whole period of HE, development and decay stages, respectively. The gray and white contours in Figures 4c and 4d denote the SST threshold and the contour of SSTs less than 27°C, respectively.

standard deviation which indicates that easterly and westerly winds intermittently occur in the frequent HE area. The statistical summary of all cases is shown in Figure 3c. During the development stage, easterly wind is weaker than its climatology with the peak frequency at −2 m/s. In contrast, strong westerly winds come during the decay stage, denoted by the increase of relative frequency of positive zonal wind component. However, the easterly winds still hold the highest relative frequency (i.e., −3 m/s) since the turning of wind direction in the decay stage does not occur in the whole HE area. Therefore, the anomaly of surface wind direction from its climatology (i.e., the presence of strong westerly wind inside HE area) can be the characteristic of the decay stage of HE in the western equatorial Pacific.

3.2. Case Study of HE030528

3.2.1. Case Selection

For the case study, we chose the HE that began on 28 May 2003 (hereafter HE030528) instead of the HE041216 introduced in *Wirasatriya et al.* [2015], based on the following two specific reasons. First, HE030528 has a single peak of HE areal size, i.e., the development and the decay stages of the HE occurred consecutively and are clearly separated. Thus, the atmospheric variation between the development and decay stages can be compared directly. Second, HE030528 can represent the general characteristics of HE in the western equatorial Pacific examined in the climatological analysis, i.e., higher solar radiation and lower wind speed during the development stage and the presence of strong westerly wind during the decay stage.

The general feature of HE030528 is described in Figure 4. HE030528 was located along the northern coast of New Guinea Island and extended to 190°E throughout the event (Figure 4a). Amplitude of HE, which is the SST subtracted from the space-time-dependent threshold described in *Wirasatriya et al.* [2015], is maximum at 0°N and 137°E. HE030528 developed from 27 to 31 May 2003 and decayed from 31 May to 11 June 2003

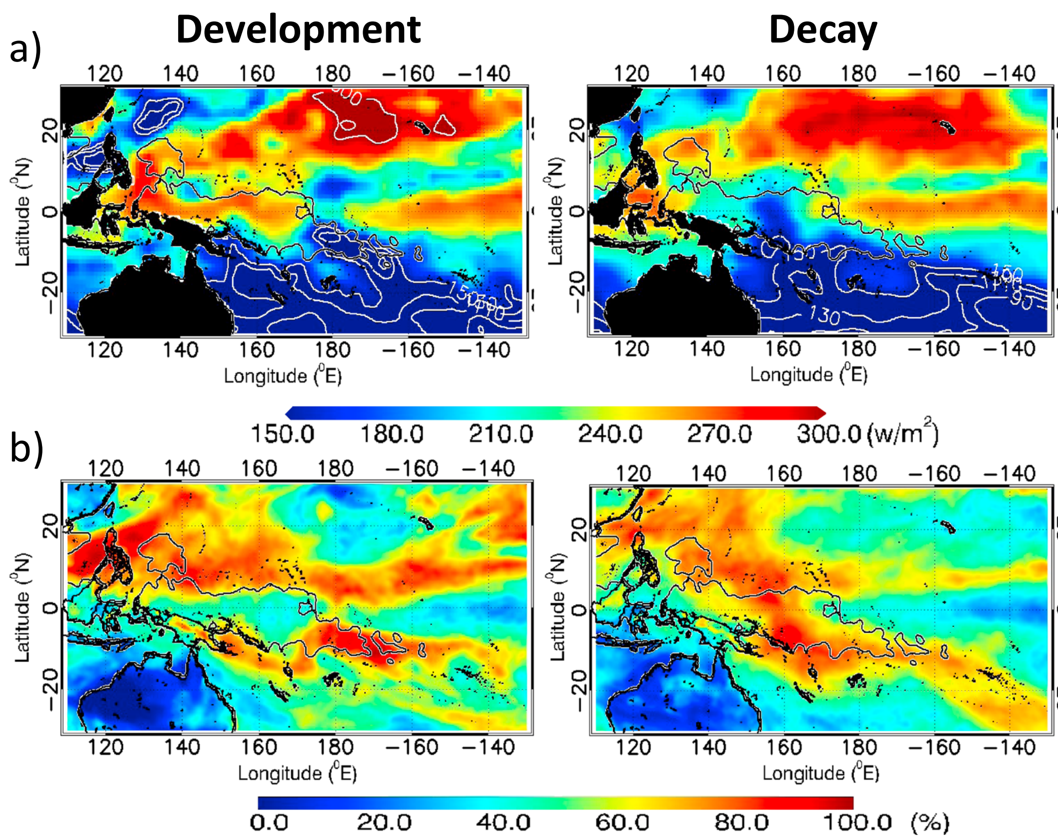

Figure 5. (a) Solar radiation and (b) total cloud cover map during the development and decay stages of HE030528. The black contour denotes the HE area. The white contour denotes the out of range solar radiation from the color bar.

(Figure 4b). The maximum areal size was 3.32×10^6 km^2. The size of HE shrank during the decay stage, leaving the high SSTs area only at the northern part of New Guinea Island.

3.2.2. Solar Radiation Variability

First, we compared the solar radiation maps between the development and decay stages of HE030528 and related them with total cloud cover maps (Figure 5). During the development stage, the high solar radiation more than 250 W/m^2 almost coincided with the HE area located along the equator from 120°E to 175°E. The high solar radiation area corresponded to the band-shaped structure of low cloud cover less than 40%. This low cloud cover band becomes the typical characteristic of HE030528. During the decay stage, the total cloud cover increased and solar radiation decreased. The high albedo of cloud may prevent solar radiation penetrating to the sea surface. Moreover, the minimum solar radiation in the HE area was detected at 5°S–5°N, 150°E–160°E, which caused the eastern part of HE to decline during the decay stage.

The vertical sections of atmosphere averaging from 155°E to 160°E shows the distinctive atmospheric features of the development and decay stages (Figure 6). Throughout the event, high-level (300–100 hPa) and low-level (950–800 hPa) clouds were dominant in the study area (Figures 6a and 6f).

During the development stage, the HE area (5°S–5°N) was denoted by the vanishing cloud at the high level and the reducing cloud at the low level (Figure 6a). The area with significantly reduced clouds corresponded to the atmospheric column with negligible convective heating rate (Figure 6b). This column was filled by the air subsidence which brought the dry air from the top of the troposphere (Figures 6c and 6d). The air subsidence was consistent with divergence at 950–800 hPa and convergence at 300–100 hPa (Figure 6e), creating double meridional circulation in the area of 17°S–0°N and 0°N–20°N. During the decay stage, the subsidence area turned back into the convection area, increasing cloud cover at the low-and high-level atmosphere (Figures 6f–6j).

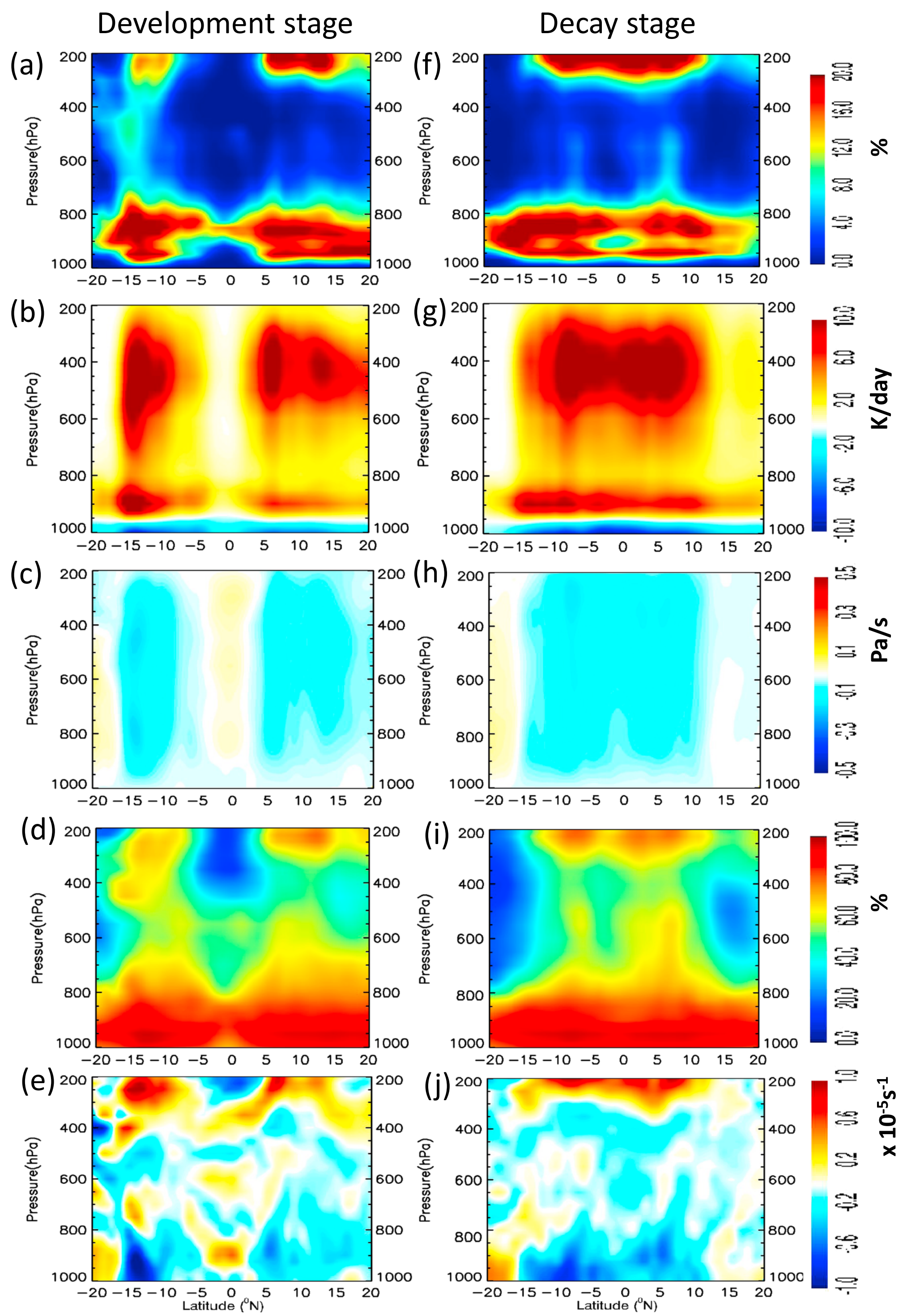

Figure 6. Vertical section of (a) cloud cover, (b) convective heating rate, (c) vertical velocity, (d) relative humidity, and (e) divergence during the development stage of HE030528 averaging from 155°E to 160°E; Figures 6f–6j are the same with Figures 6a–6e for the decay stage. HE area is located around 5°S to 5°N.

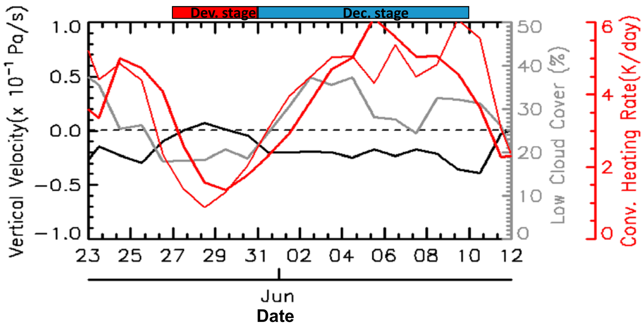

Figure 7. The time series of vertical velocity, convective heating rate, and low cloud cover (850 to 1100 hPa) at 155°E–160°E, 5°S–5°N. Mean convective heating rate is taken at 1000–950 hPa (lower) denoted by thick line, and 950–900 hPa (upper) denoted by thin line, and mean vertical velocity is at 1000–900 hPa.

Focusing on the low-level atmosphere (1000–700 hPa), we found that the convection during the development stage of HE030528 was limited to the lower level only. Despite being suppressed by the subsidence at the upper troposphere, the convection process still occurred and could produce thin cloud layer at around 850 hPa (Figures 6a and 7). This is probably caused by the existence of temperature inversion layer at around 800 hPa (Figure 8) that protects the air subsidence that penetrates to the surface level. An inversion acts like a lid, keeping convective overturning of the higher atmosphere from penetrating to the surface layer. In the decay stage, the inversion layer reduced as the convection increased.

3.2.3. Surface Wind Variability of HE030528

We investigated the surface wind variability during the development and decay stages of HE. Figure 9 shows that the area with low wind speed coincided with the HE area during the development stage. The SLP was relatively uniform (≈1010 hPa), causing the low SLP gradient magnitude in the HE area. Lower SLP was detected at the eastern side, at around 10°S, 180°E. During the decay stage, the low SLP area moved to the northern coast of Solomon Islands.

The geographical location of the Solomon Islands, Bougainville Island, New Britain Island, and New Ireland Island creates a terrestrial gap, located between the western tip of Bougainville Island and the eastern tip of New Ireland Island. The westward moving of low SLP during the decay stage increased the SLP difference between the area at the southside of the gap and the area at the northern coast of Solomon Islands, generating strong wind through the gap to the low SLP area. Therefore, land topography becomes an important factor for the decaying mechanisms of HE030528. Furthermore, the strong winds in this area may also reduce high SST area of HE030528 during the decay stage as described in section 3.2.1 (Figure 4d).

The variation of zonal wind component gives more influence to the HE development and decay. In HE030528, the meridional wind component was relatively stable during the development and decay stages of HE. Weak and negative zonal wind component (i.e., easterly wind) was observed during the development stage and then turned into positive (i.e., westerly wind) and increased speed during the decay stage (Figure 10). Thus, the occurrence of westerly wind triggered the decay of HE030528.

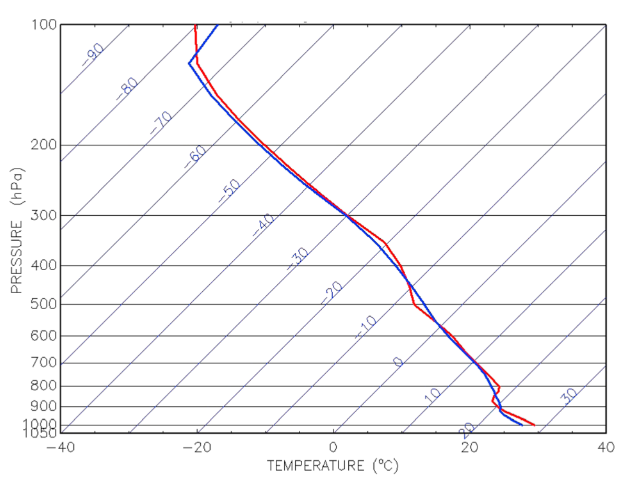

Figure 8. Skew T, Log P diagram of air temperature at 0°N, 157°E. Red curve represents development stage (29 May 2003) and blue curve represents decay stage (7 June 2003).

3.2.4. The Role of Surface Wind on Controlling the Solar Radiation Variability

The atmospheric boundary layer controls the convection process to the top of troposphere [e.g., *Sherwood*, 1999; *Tompkins*, 2001]. The present study indicates that surface wind speed determines the surface evaporation and the moisture supply for the upper atmosphere; surface divergence determines the vertical air motion. Figure 11a shows that as

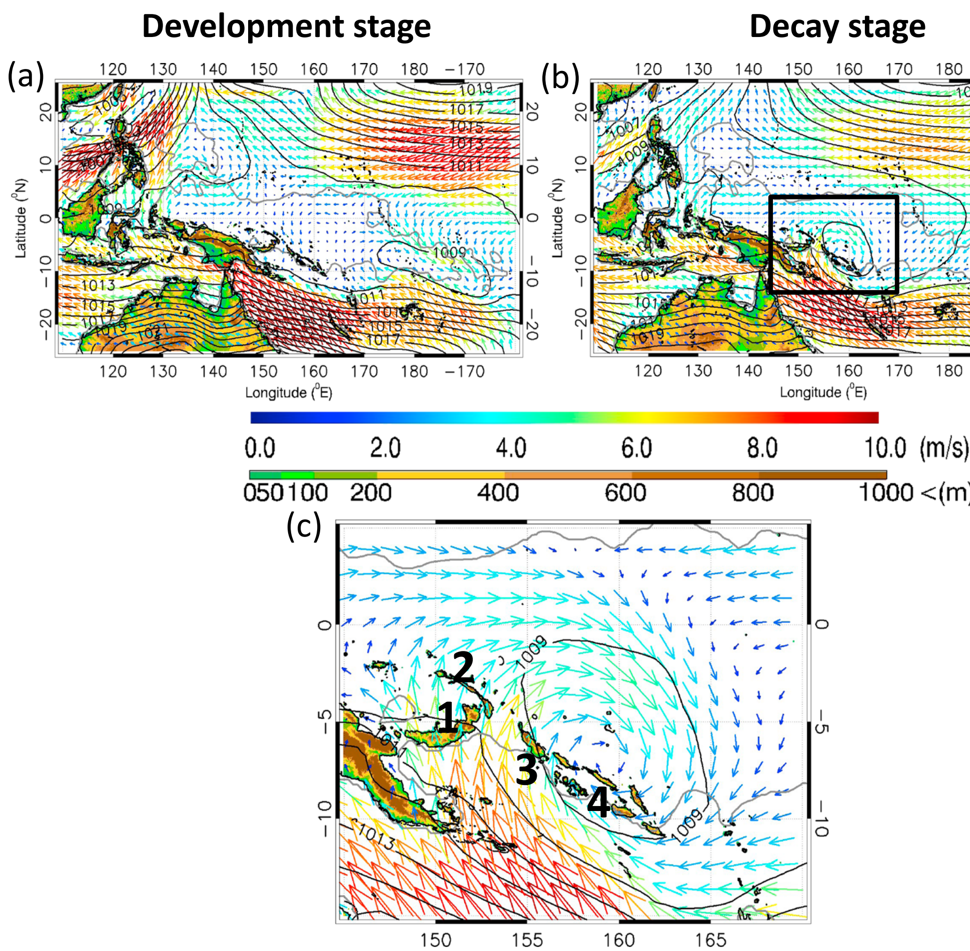

Figure 9. Surface wind vector overlaid by SLP contour during (a) the development and (b) decay stages of HE20030528. (c) The zoomed area of black square in Figure 9b. The numbers 1, 2, 3, and 4 denote New Britain Island, New Ireland Island, Bougainville Island, and Solomon Islands, respectively.

the wind speed decreased during the development stage of HE030528, the surface evaporation also decreased and the weakening surface convergence reduced the upward motion strength. The existence of a thermal inversion layer during the development stage also may contribute to the reduction of upward motion. At the upper atmosphere, the variation of relative humidity was consistent with the surface evaporation and the variation of vertical velocity was consistent with surface convergence (Figure 11b). On 25 May 2003, when the surface convergence and surface evaporation started to decrease, the convection process and relative humidity at the upper atmosphere also started to decrease. On the other hand, dry air from the top of the troposphere sank and suppressed the convection. Then, solar radiation increased as a result of the suppressed convection. During the decay stage, surface wind

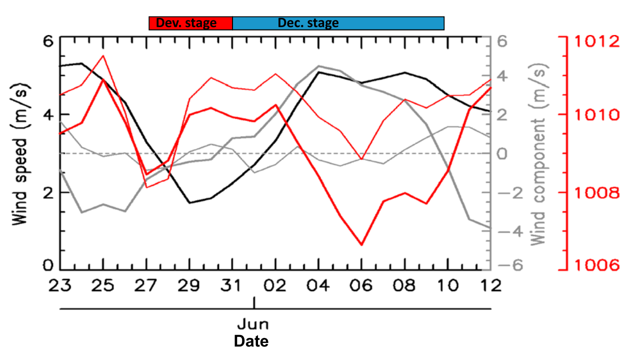

Figure 10. The time series of wind speed, wind component, and SLP. Wind component is sampled at 145°E–165°E, 5°S–5°N. Thick and thin lines denote U and V components, respectively. SLP is sampled at the southside of the gap (150°E–155°E, 10°S–5°S) denoted by thin line, and at the northern coast of the Solomon Islands (158°E–163°E,7°S–2°S) denoted by thick line.

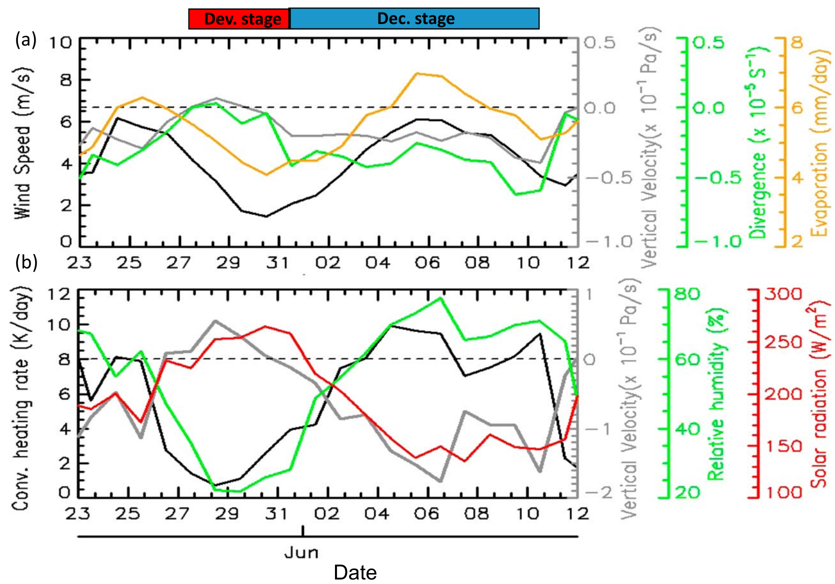

Figure 11. The time series of atmospheric parameters at 155°E–160°E, 5°S–5°N. (a) Wind speed, evaporation, and divergence at the surface level, and vertical pressure velocity at lower troposphere (1000 hPa–900 hPa). (b) Convective heating rate, vertical pressure velocity, relative humidity at upper troposphere (400 hPa–200 hPa), and solar radiation. Surface divergence is calculated from surface wind.

speed increased, surface convergence became stronger, and convection process began to reduce solar radiation. Therefore, surface wind plays an important role on solar radiation variability during the HE process. Thus, this result supports surface wind as the key factor for the HE occurrence as mentioned in *Wirasatriya et al.* [2015].

4. Discussion

4.1. Comparison to the Previous High-SST Study

The "remote convection" mechanism for the HE generation in the western equatorial Pacific has been previously described by *Qin and Kawamura* [2010]. However, there is a significant difference from the "remote convection" found in this study. *Qin and Kawamura* [2010] divided the region associated with HE0611 into two, i.e., HE0611-East and HE0611-West. Using the cloud motion wind and cloud cover data obtained from geostationary satellite measurements, they found that the deep convection over the area of HE0611-East caused the air subsidence over the area of HE0611-West and induced the HE there. The occurrence of HE0611-East was supported by the subsurface positive temperature anomaly associated with the El Niño. Thus, their result indicates zonal circulations through HE0611-East and HE0611-West.

In contrast, the present study shows the meridional circulation of the "remote convection" mechanism during the development of HE030528. The suppressed convection above the HE area was the result of the deep convection from the areas on the north (5°N–20°N) and south (17°S–5°S) (Figure 4b). *Rasmusson and Wallace* [1983] stated that surface wind convergence associated with the ascending branch of the Walker circulation is the typical characteristic of the western equatorial Pacific. In this study, this convergence/convection areas along the equator turned into subsidence areas during the development of HE030528, creating the tropospheric "flywheel effect" which means that the subsidence area along the equator was flanked by the convection areas on the north and south.

Typical features of band-shaped structure of low cloud cover during the development stage of HE030528 did not occur for all HE cases. We have confirmed that only 20 HEs have the characteristic of low cloud cover band during the development stage. Nevertheless, the rest of the cases still show the lower cloud cover during the development stage than the decay stage. Thus, the occurrence of the double meridional circulation is not the general characteristic of the development stage of HE in the western equatorial Pacific. Furthermore, we also demonstrated the role of land topography and the westward movement of low pressure system for the

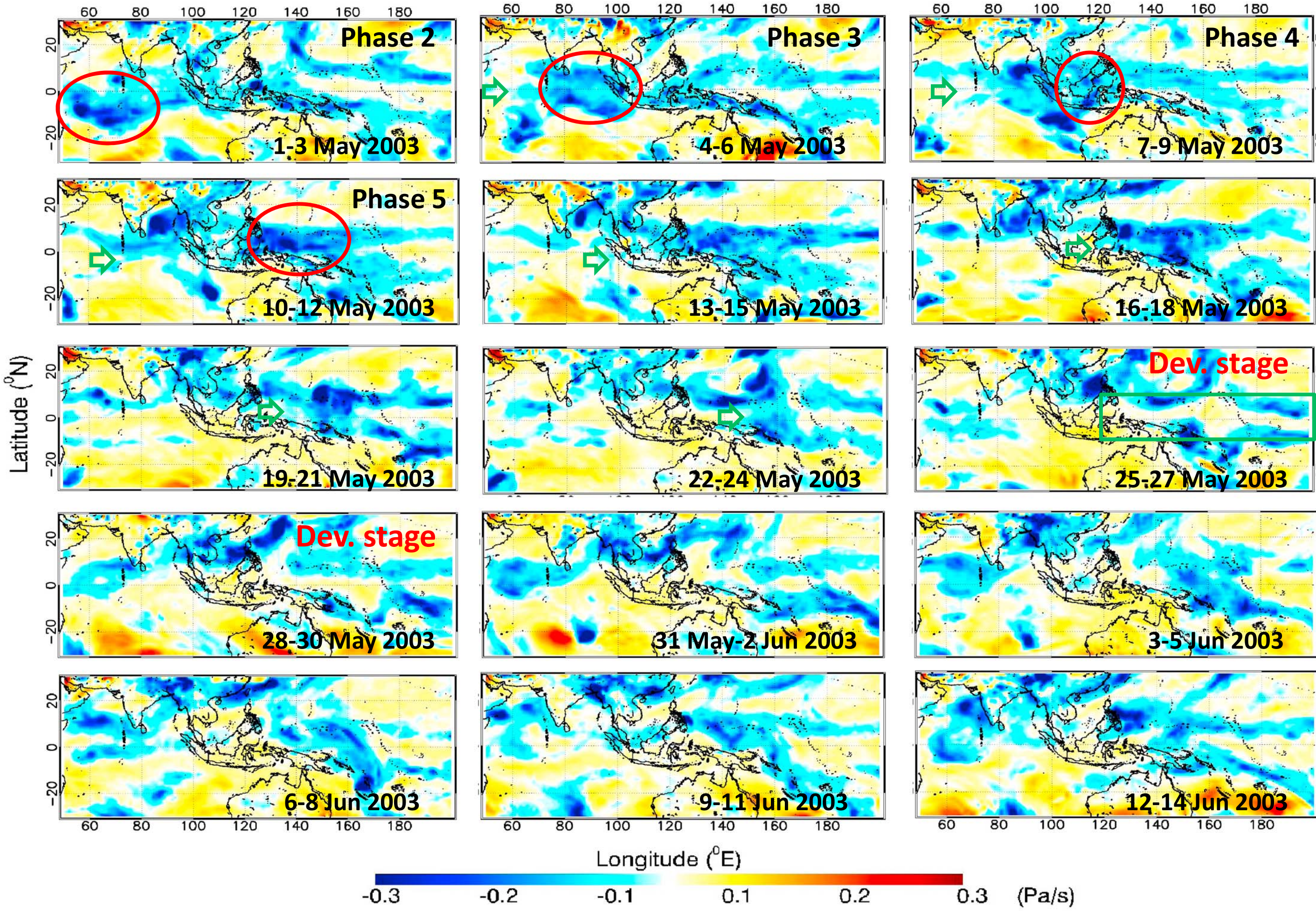

Figure 12. The time series of pressure vertical velocity map at 600 hPa. Red circle denotes the strong upward motion (active phase) of the MJO and green arrow denotes the suppressed phase of the MJO. Green box denotes the air subsidence band along the equator.

decay of HE030528 which was absent for the mechanism of HE0611. This also becomes the typical characteristic of several HEs in the western equatorial Pacific since we found 19 cases among 71 HEs. Thus, the mechanisms on how solar radiation increases during development stage of HE and how strong westerly wind occurs during the decay stage of HE cannot be generalized. The analysis of other HE cases may found different processes and these tasks are potential for future studies.

Tompkins [2001] addressed the importance of surface latent heat flux that guides the convection toward the high SST areas, and finally reducing SSTs. Moreover, *Chen and Qin* [2016] emphasized the strong atmospheric instability that induces the convection toward the high SST areas. In the case of HE030528, we propose a hypothesis that those processes may be enhanced due to the westerly wind, increasing evaporation as well as latent heat flux. If so, convection was reactivated and this became the end stage of HE030528. The relation between convection and westerly wind in the western equatorial Pacific has been reported by *Kiladis et al*. [1994] who provided the evidence that the convection with the duration time of 6 to 30 days often occurs in conjunction with strong westerly flows. In the case of HE030528, westerly wind might be caused by the westward propagation of low pressure system interacted with the land surface topography of New Britain Island, New Ireland Island, Bougainville Island, and Solomon Islands. Further investigations are needed to examine the relation between the decay of HE and the westward propagation of the low pressure system.

Considering other high SST studies, we can note that there are two critical thresholds of high SST which correspond to the tropical deep convection. First is 27°C. *Su et al*. [2006] found that after 27°C, deep convection sharply increases, with the increase of SST. The moistening of the upper troposphere by deep convection

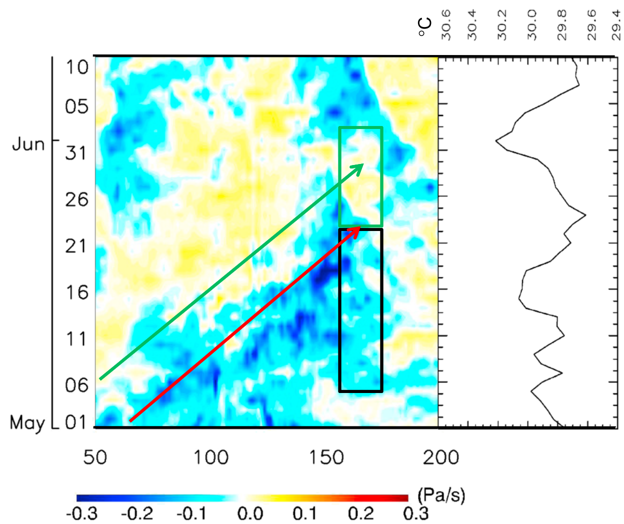

Figure 13. Hovmöller diagram (5°S–5°N) of vertical pressure velocity at 600 hPa and time series of SST at 150°E–170°E in 2003. Red and green arrows denote the eastward propagation of deep convection and air subsidence, respectively. Black square denotes the convective period of the western equatorial Pacific. Green square denotes subsidence air period indicating the development stage of HE030528 in the western equatorial Pacific.

leads to an enhanced positive water vapor feedback, about 3 times that implied solely by thermodynamics. However, due to the limited spatial and temporal SST data (i.e., monthly and 8° × 4°), they cannot observe the SSTs higher than 30°C. Second is 30°C. A series of HE studies from *Qin et al*. [2007] to the present study have shown that after ~30°C, convection decreases with the increase of SST which imply that to reach SSTs higher than ~30°C, clear sky condition is needed. In case of HE0611-East, clear sky condition above the HE area was influenced by El Niño [*Qin et al*., 2008]. In the present study, although the evidences of clear sky condition during the development stage of HE030528 has been provided, the mechanisms on how it was created still leave questions. For example, is the formation of low cloud cover band during the development stage a solely self-regulating system related to the weakening of surface convergence? Or are there any external forces that influence its formation? In the next section, the possible relation between the development stage of HE and MJO is discussed.

4.2. Possible Relation to MJO

On the larger scale, we can see the possible relation between the development of HE030528 and the propagation of MJO. MJO is characterized by a strong deep convection moving eastward and high precipitation (active phase), flanked at both east and west by regions of weak deep convection and low precipitation (suppressed phases). The zonal circulations connect both phases, extending vertically through the entire troposphere [*Zhang*, 2005]. The track of the eastward propagation of strong deep convection from Indian Ocean to Pacific Ocean was identified by *Wheeler and Hendon* [2004] and named it as phases 1 until 8. In the present study, the eastward propagation of strong deep convection is detected by the upward air motion moving along the equator (Figure 12). On 1–3 May 2003, strong convection appeared in the Indian Ocean at 50°E to 80°E indicating phase 2 of MJO. Phase 3 occurred on 4–6 May 2003 indicated by strong convection at 70°–110°E. Phase 4 was denoted by the arrival of strong convection at Indonesian maritime continent that occurred on 7–9 May 2003. The appearance of strong convection signal was ended at the western equatorial Pacific on 10–12 May 2003 corresponding to phase 5. After that, we cannot see the eastward convection signal moving along the equator. As explained by *Zhang* [2005], the convection signal of MJO normally vanishes at the eastern equatorial Pacific.

The active phase of MJO is followed by the suppressed phase with the eastward propagation of air subsidence along the equator. In Figure 12, the suppressed phase of MJO is denoted by the green arrow. During the development stage of HE030528 (25–30 May 2003), the suppressed phase of the MJO arrived at the western equatorial Pacific, met with the branch of Intertropical Convergence Zone and South Pacific Convergence Zone creating the band-shaped structure of subsidence along the equator. This band-shaped structure of air subsidence prevented the cloud formation as described in the previous section and then increased the incoming solar radiation. Thus, the high solar radiation during the development stage of HE030528 might be affected by the MJO. After 5 June 2003, western equatorial Pacific turned back into convective area.

We can confirm that the suppressed phase of MJO coincide with the development stage of HE. Hovmöller diagram (Figure 13, left) also shows that the area of HE030528 (150°E to 170°E) had strong convective period from 6 to 22 May 2003 (black square), turned into the period of subsidence air from 23 May to 1 June 2003 (green square) and then turned back into the convective period. This turning condition is related to the transition from the active phase to the suppressed phase of MJO. The prominent signal of the active phase of MJO was indicated by the eastward propagation of the deep convection of about 4.6 m/s and vanished on 23 May 2003 at around 150°E to 170°E (red arrow). The propagation of the deep convection was followed by the propagation of air subsidence (green arrow) which caused occurrence of air subsidence in the area of HE030528.

The air subsidence occurred during the development stage of HE030528. The effect of MJO is clearly seen from the increasing SST from 23 May 2003 to 1 June 2003 corresponding to the development stage of HE030528 (Figure 13, right). The amplitude of this increasing SST was about 0.5°C which is twice larger than the SST variation produced by the MJO provided by *Shinoda et al*. [1998]. However, this interaction should be investigated further in future studies by investigating the physical process behind the relation between the suppressed phase of MJO and the development stage of HE; this relation may be just coincidence. Moreover, we also consider that the eastward propagation of the suppressed phase of MJO during the development stage and the westward propagation of low pressure system during the decay stage are two independent systems. On the other hand, the relationship between the MJO and the tropical cyclone as well as the low pressure system has been well documented by *Liebmann et al*. [1994]. Thus, further investigation of the relationships among HE, MJO, and the tropical cyclone will be the potential subject for future works.

5. Conclusions

The analysis of atmospheric structure during the development and decay stage of HE are concluded as follows.

1. Climatological analysis shows that the development stage of HE is indicated by higher solar radiation than its climatology and lower wind speed than the decay stage. The decay stage of HE is characterized by the occurrence of strong westerly wind.
2. The suppressed convection above the HE030528 area resulted from the deep convection from the area outside the HE. The suppressed convection then created low cloud cover band along the HE area increasing solar radiation during the development stage. Thus, the theory of "remote convection" is supported for the HE formation mechanisms.
3. Strong wind induced by the large SLP gradient between the southside of the terrain gap and the northern coast of the Solomon Islands contributed to the decay of HE030528.
4. Surface wind influenced the variability of solar radiation during the occurrence of HE030528 by controlling the water vapor supply in the upper troposphere through surface evaporation and surface convergence variation. Thus, surface wind played as the key factor for HE030528.
5. HE030528 can represent the features of HE in the western equatorial Pacific in terms of high solar radiation during the development stage and strong westerly wind during the decay stage. However, the mechanisms on how solar radiation increase during development stage of HE and how strong westerly wind occurs during the decay stage cannot be generalized since they occurred for less than 30% of total HE cases. These mechanisms may be substantial for understanding the formation of high SSTs in the equatorial region, since they have never been observed in the previous HE studies.

Acknowledgments
NGSST-O-Global-V2.0a is produced by Center for Atmospheric and Oceanic Studies, Tohoku University, Japan. Contact for data inquiry and request is Kohtaro Hosoda (hosoda@ocean.caos.tohoku.ac.jp). JRA-55 and ISCCP-FD data were provided by the Japan Meteorological Agency and courtesy of the NASA Goddard Institute for Space Studies, respectively. GTOPO30 data are available from the U.S. Geological Survey. The first author is thankful to the Directorate General of Higher Education, Indonesian Republic, for the PhD scholarship and Susan R Vulpas for English improvement.

References

Arking, A., and D. Ziskin (1994), Relationship between clouds and sea surface temperatures in the western tropical Pacific, *J. Clim.*, *7*, 988–1000.

Chen, G., and H. Qin (2016), Strong ocean-atmosphere interactions during a short-term hot event over the western Pacific warm pool in response to El Niño, *J. Clim.*, *29*(10), 3841–3865, doi:10.1175/JCLI-D-15-0595.1.

Hosoda, K. (2013), Empirical method of diurnal correction for estimating sea surface temperature at dawn and noon, *J. Oceanogr.*, *69*, 631–646, doi:10.1007/s10872-013-0194-4.

Hosoda, K. (2015), Global space-time scales for day-to-day variations of daily-minimum and diurnal sea surface temperatures: Their distinct spatial distribution and seasonal cycles, *J. Oceanogr.*, *72*, 281–298, doi:10.1007/s10872-015-0327-z.

Hosoda, K., and F. Sakaida (2015), Development of daily-minimum sea surface temperature data set based on microwave and visible/infrared measurements from space, Proc. 30th Int. Symp. on Space Technology and Science (2015-n-37), Kobe, Japan. [Available at http://archive.ists.or.jp/upload_pdf/2015-n-37.pdf.]

Kawamura, H., H. Qin, and K. Ando (2008), In-situ diurnal sea surface temperature variations and near-surface thermal structure in the tropical Hot Event of the Indo-Pacific warm pool, *J. Oceanogr.*, *64*, 847–857.

Kiladis, G. N., G. A. Meehl, and K. M. Weickmann (1994), Large-scale circulation associated with westerly wind bursts and deep convection over the western equatorial Pacific, *J. Geophys. Res.*, *99*, 18,527–18,544, doi:10.1029/94JD01486.

Kobayashi, S., et al. (2015), The JRA-55 reanalysis: General specifications and basic characteristics, *J. Meteor. Soc. Jpn.*, *93*(1), 5–48, doi:10.2151/jmsj.2015-001.

Liebmann, B., H. H. Hendon, and J. D. Glick (1994), The relationship between tropical cyclone of the western Pacific and Indian oceans and the Madden–Julian Oscillation, *J. Meteor. Soc. Jpn.*, *72*(3), 401–412.

Qin, H., and H. Kawamura (2009a), Surface heat fluxes during hot events, *J. Oceanogr.*, *65*, 605–613.

Qin, H., and H. Kawamura (2009b), Atmosphere response to a hot SST event in November 2006 as observed by AIRS instrument, *Adv. Space Res.*, *44*, 395–400, doi:10.1016/j.asr.2009.03.003.

Qin, H., and H. Kawamura (2010), Air-sea interaction throughout the troposphere over a very high sea surface temperature, *Geophys. Res. Lett.*, *37*, L01704, doi:10.1029/2009GL041685.

Qin, H., H. Kawamura, and Y. Kawai (2007), Detection of hot event in the equatorial Indo-Pacific warm pool using advanced satellite sea surface temperature, solar radiation, and wind speed, *J. Geophys. Res.*, *112*, C07015, doi:10.1029/2006JC003969.

Qin, H., H. Kawamura, F. Sakaida, and K. Ando (2008), A case study of the tropical hot event in November 2006 (HE0611) using a geostationary meteorological satellite and the TAO/TRITON mooring array, *J. Geophys. Res.*, *113*, C08045, doi:10.1029/2007JC004640.

Ramanathan, V., and W. Collins (1991), Thermodynamic regulation of ocean warming by cirrus clouds deduced from observations of the 1987 El Niño, *Nature*, *351*, 27–32.

Rasmusson, E. M., and J. M. Wallace (1983), Meteorological aspects of the E1 Niño/Southern Oscillation, *Science*, *222*, 1195–1202.

Sherwood, S. C. (1999), Convective precursors and predictability in the tropical western Pacific, *Mon. Weather Rev.*, *127*, 2977–2991.

Shinoda, T., H. Hendon, and J. Glick (1998), Intraseasonal variability of surface fluxes and sea surface temperature in the tropical western Pacific and Indian Oceans, *J. Clim.*, *11*, 1685–1702.

Su, H., W. G. Read, J. H. Jiang, J. W. Waters, D. L. Wu, and E. J. Fetzer (2006), Enhanced positive water vapor feedback associated with tropical deep convection: New evidence from Aura MLS, *Geophys. Res. Lett.*, *33*, L05709, doi:10.1029/2005GL025505.

Tompkins, A. M. (2001), On the relationship between tropical convection and sea surface temperature, *J. Clim.*, *14*, 633–637.

Waliser, D. E., and N. E. Graham (1993), Convective cloud systems and warm-pool sea-surface temperatures: Coupled interactions and self-regulation, *J. Geophys. Res.*, *98*, 12,881–12,893, doi:10.1029/93JD00872.

Wallace, J. M. (1992), Effect of deep convection on the regulation of tropical sea surface temperature, *Nature*, *357*, 230–231.

Wheeler, M., and H. H. Hendon (2004), An all-season real-time multivariate MJO index: Development of an index for monitoring and prediction, *Mon. Weather Rev.*, *132*, 1917–1932.

Wirasatriya, A., H. Kawamura, T. Shimada, and K. Hosoda (2015), Climatology of hot events in the western equatorial Pacific, *J. Oceanogr.*, *71*, 77–90, doi:10.1007/s10872-014-0263-3.

Zhang, C. (2005), Madden-Julian Oscillation, *Rev. Geophys.*, *43*, RG2003, doi:10.1029/2004RG000158.

Zhang, Y. C., W. B. Rossow, A. A. Lacis, V. Oinas, and M. I. Mishchenko (2004), Calculation of radiative fluxes from the surface to top of atmosphere based on ISCCP and other global data sets: Refinements of the radiative transfer model and the input data, *J. Geophys. Res.*, *109*, D19105, doi:10.1029/2003JD004457.